Archival Report

Biological Psychiatry: GOS

# Modeling Intrahippocampal Effects of Anterior Hippocampal Hyperactivity Relevant to Schizophrenia Using Chemogenetic Excitation of Long Axis–Projecting Mossy Cells in the Mouse Dentate Gyrus

James P. Bauer, Sarah L. Rader, Max E. Joffe, Wooseok Kwon, Juliana Quay, Leann Seanez, Chengwen Zhou, P. Jeffrey Conn, and Alan S. Lewis

## ABSTRACT

**BACKGROUND:** The anterior hippocampus of individuals with early psychosis or schizophrenia is hyperactive, as is the ventral hippocampus in many rodent models for schizophrenia risk. Mossy cells (MCs) of the ventral dentate gyrus (DG) densely project in the hippocampal long axis, targeting both dorsal DG granule cells and inhibitory interneurons. MCs are responsive to stimulation throughout hippocampal subfields and thus may be suited to detect hyperactivity in areas where it originates such as CA1. Here, we tested the hypothesis that hyperactivation of ventral MCs activates dorsal DG granule cells to influence dorsal hippocampal function.

**METHODS:** In CD-1 mice, we targeted dorsal DG-projecting ventral MCs using an adeno-associated virus intersectional strategy. In vivo fiber photometry recording of ventral MCs was performed during exploratory behaviors. We used excitatory chemogenetic constructs to test the effects of ventral MC hyperactivation on long-term spatial memory during an object location memory task.

**RESULTS:** Photometry revealed that ventral MCs were activated during exploratory rearing. Ventral MCs made functional monosynaptic inputs to dorsal DG granule cells, and chemogenetic activation of ventral MCs modestly increased activity of dorsal DG granule cells measured by c-Fos. Finally, chemogenetic activation of ventral MCs during the training phase of an object location memory task impaired test performance 24 hours later, without effects on locomotion or object exploration.

**CONCLUSIONS:** These data suggest that ventral MC activation can directly excite dorsal granule cells and interfere with dorsal DG function, supporting future study of their in vivo activity in animal models for schizophrenia featuring ventral hyperactivity.

https://doi.org/10.1016/j.bpsgos.2021.04.005

Several groups have reported that the anterior hippocampus (HPC) in individuals with early psychosis or schizophrenia is reduced in volume (1–5) and hyperactive at baseline (1,6–9). Anterior hyperactivity is associated with cognitive deficits and impaired recruitment or habituation of the anterior HPC during cognitive tasks (6,10–14). However, causal relationship between anterior HPC activity and deficits in learning and memory remains unclear (15).

Many rodent models with genetic or developmental insults for modeling schizophrenia etiology also exhibit hyperactivity in the ventral HPC (vHPC), the rodent analog of the human anterior HPC [reviewed in (16,17)]. Work in these models suggests that vHPC hyperactivity drives aberrant dopamine neurotransmission through extrahippocampal projections to nucleus accumbens, resulting in positive symptoms of psychosis [reviewed in (18)]. vHPC interactions with the medial prefrontal cortex are also important for spatial working memory (19–23), and synchrony deficits between these brain regions in rodent models for schizophrenia correlate with spatial working memory impairment (22). However, causal links between vHPC hyperactivity and cognitive deficits remain sparse. Wolff *et al.* (24) used optogenetics to directly demonstrate that vHPC hyperactivation impairs performance on the spatial novelty preference test of HPC-dependent short-term memory. This work is particularly important because it suggested that the observed cognitive deficit is independent of the hyperdopaminergic state and associated phenotypes. This form of working memory involves projections both extrahippocampally to medial prefrontal cortex and nucleus reuniens and intrahippocampally to the dorsal HPC (dHPC), the rodent equivalent of the human posterior HPC. Patients with early psychosis or schizophrenia largely do not demonstrate significant

SEE COMMENTARY ON PAGE 83





ISSN: 2667-1743

posterior HPC hyperactivity (1,6), but posterior HPC activation is reduced during cognitive tasks examining fine-grained spatial relationships (12). Understanding how ventral and dorsal aspects of the HPC interact through intrahippocampal long axis circuitry and whether hyperactivity of this circuitry in the vHPC might influence dHPC physiology and function would further the understanding of potential downstream consequences of anterior HPC hyperactivity in patients with schizophrenia.

To model the functional consequences of hyperactive long-distance projections originating in the ventral half of the HPC, here we focus on ventral mossy cells (vMCs), which are glutamatergic neurons with cell bodies in the dentate gyrus (DG) hilus (25,26). Ventral MCs send long-distance excitatory projections to the DG bilaterally, where they target both granule cell dendrites in the inner molecular layer (IML) and granule cell–inhibiting interneurons across the entire longitudinal HPC axis (27–30). While vMC activation results in excitation of both dHPC granule cells and interneurons in vivo (31), the net effect of feedforward excitation and disynaptic inhibition on dHPC granule cell activity has varied from weak (32) to strong (33), using different techniques. Functionally, optogenetic inhibition of vMCs during the training but not the testing phase of a long-term object location memory (OLM) task impairs spatial memory (31), again suggesting involvement of the dHPC, given its importance in long-term spatial memory (34,35). MCs are sensitive to low levels of activity throughout HPC subfields (36), including in area CA1 where hyperactivity in psychosis is observed early (1,8), and thus are plausible candidates to be functionally responsive to HPC hyperactivity. In this study, we used vMCs as a longitudinal HPC model circuit, quantified vMC in vivo activity during environmental exploration, characterized their connectivity with target dorsal DG (dDG) granule cells, and determined the consequences of chemogenetic vMC hyperactivation in a long-term spatial memory task involving dHPC function.

## METHODS AND MATERIALS

Detailed methods are reported in the Supplement.

### Animals

CD-1 mice (Charles River Laboratories, Wilmington, MA; age at delivery: 6–8 weeks) were acclimated to the vivarium for at least 1 week. Male and female mice were used for all chemogenetic behavior studies, whereas only male mice were used for fiber photometry recordings. Studies were not powered to detect sex differences; however, the sex of each mouse is displayed in behavioral data plots. Outbred mice were used, because recent work suggests that they do not display significantly greater behavioral variability than inbred strains and may provide greater generalizability for translational research (37). All mice were group housed except for cannula-implanted mice, which were single housed. Mice were housed under standard conditions with a 12-hour light/dark cycle (lights on at 6:00 AM), with food and water available ad libitum. The Vanderbilt Institutional Animal Care and Use Committee approved all procedures.

### Drugs

Clozapine N-oxide (CNO)-free base was provided by the National Institute of Mental Health Chemical Synthesis and Drug Supply Program, dissolved in 0.5% dimethyl sulfoxide in saline, and injected intraperitoneally (i.p.). For slice electrophysiology, CNO dihydrochloride was purchased from Hello Bio (Princeton, NJ).

### Adeno-associated Viruses

AAV (adeno-associated virus) particles (Addgene, Watertown, MA) used, preparation serotypes, and titers (genome copies [GC]/mL) were AAV.pgk.Cre (retrograde, $9.3 \times 10^{12}$ GC/mL), pAAV.Syn.Flex.GCaMP6f.WPRE.SV40 (AAV1, $1.9 \times 10^{13}$ GC/mL) (38), pAAV-hSyn-DIO-mCherry (AAV8, $2.6 \times 10^{13}$ GC/mL), pAAV-hSyn-DIO-hM3D(Gq) (AAV8, $2.0 \times 10^{13}$ GC/mL) (39), pENN.AAV.hSyn.Cre.WPRE.hGH (AAV1, $1.9 \times 10^{13}$ GC/mL), and pAAV-EF1a-double floxed-hChR2(H134R)-mCherry-WPRE-HGHpA (AAV8, $1.9 \times 10^{13}$ GC/mL).

### Stereotaxic Surgery and Viral Infusion

Under inhaled isoflurane anesthesia, mice were mounted in a stereotaxic frame, and AAV (0.2–0.4 μL, depending on brain region) was infused at a rate of 50 nL/min using a 2-μL syringe (Hamilton, Reno, NV). Target coordinates: 1) dorsal DG: anterior/posterior (AP): −1.94 mm, medial/lateral (ML): 1.20 mm left, dorsal/ventral (DV): −2.50 mm; 2) ventral DG hilus: AP: −3.40 mm, ML: ±3.00 mm, DV: −3.50 mm. Fiber photometry cannulas were targeted to the same coordinates as ventral DG hilus and cemented in place with C&B-Metabond (Parkell, Edgewood, NY). Mice were housed for at least 3 weeks before experimentation to allow for viral expression. Targeting was confirmed by fluorescence microscopy. Mice with either unilateral or bilateral vMC expression were included in behavioral analyses because of extensive bilateral projections.

### Fluorescent Immunostaining, Microscopy, and Cell Counting

Primary antibodies for 40-μm free-floating sections were mouse anti-calretinin (MAB1568; Millipore, Burlington, MA) (40) and rabbit anti-c-Fos (226 003; Synaptic Systems, Göttingen, Germany) (41), both diluted 1:1000. Images were acquired with either a widefield or confocal microscope. Quantitative cell counting was performed blinded from confocal images.

### Electrophysiology

To validate DREADD (designer receptor exclusively activated by designer drugs) activation of vMCs, mice were rapidly decapitated under deep isoflurane anesthesia, and 300-μm horizontal sections containing the vDG were prepared in *N*-methyl-D-glucamine cutting solution and recorded in artificial cerebrospinal fluid. Hilar MCs were identified by mCherry expression, patched to obtain whole-cell access, and voltage-clamped at −75 mV while 10-μM CNO was perfused in the bath. The mean of the holding current was quantified before and after CNO perfusion using pClamp 10.4 software (Axon Instruments, Union City, CA). For optogenetic activation of vMC terminals in dDG, brain slices were prepared as previously described (42,43). Whole-cell patch-clamp recordings were made from dDG granule cells, and slices were continuously superfused with artificial cerebrospinal fluid. Current-

clamp mode was used to record action potentials. Blue laser light (475-nm wavelength, 5-ms pulse duration, 20 Hz, 1-s duration) was delivered through a fiberoptic cable to stimulate channelrhodopsin-expressing vMC axon terminals. In both sets of experiments, recordings were acquired with a Multiclamp 700B amplifier (Molecular Devices, Sunnyvale, CA), filtered at 2 kHz and digitized at 10 kHz.

## Behavioral Studies

**General.** Mice were habituated to the testing room (approximately 200 lux) for at least 1 hour before testing. Testing occurred between 9:00 AM and 5:00 PM. Experimental and control groups were tested on the same days, and all tests were videotaped. Vehicle or CNO was injected i.p. 30 minutes before the start of behavioral assays.

**Open Field Test.** Mice were placed into the center of a 61 cm × 61 cm square arena for 10 minutes. Distance traveled, time spent in arena center, and number of center entries were quantified using ANY-maze version 6.1 (Stoelting, Wood Dale, IL). Rearing, defined as standing upright on hind legs, was quantified manually by an observer blinded to treatment group.

**OLM Test.** OLM test was performed largely as described previously (44). Mice were handled for about 2 minutes daily for 5 days, followed by 5 minutes of habituation daily in an empty 61 cm × 61 cm open field containing spatial cues on the wall for 6 days (final 2 days of handling were combined with habituation). The next day, mice underwent a training session, during which they were placed in the same arena now containing 2 identical 500-mL glass bottles spaced approximately 30 cm apart and allowed to explore the arena for 10 minutes. Bottles were cleaned with dilute alcohol solution between mice. Twenty-four hours later, mice were returned to the same arena for a 5-minute testing session, where one bottle remained in the same location and the other bottle was moved approximately 40 cm to a novel location. The side from which the bottle was moved was counterbalanced across mice. Time spent exploring each bottle was quantified from video by blinded observers. Only time during which mice directly explored the object (approximately 0–2 cm away) and were not rearing was counted (44). Discrimination index (DI) for the testing session was quantified as (time exploring novel object – time exploring familiar object)/(total time exploring both objects), with DI for training session calculated with future novel and future familiar objects used in the above equation. Mice demonstrating an initial side preference during the training session (DI > 0.20) (31) were removed from the analysis ($n$ = 2 mCherry, 3 hM3Dq).

**c-Fos Expression.** Mice were habituated to the testing room for >2 hours, administered CNO or vehicle i.p., and transcardially perfused 90 minutes later.

## Fiber Photometry

Photometry was performed from male mice implanted with photometry cannulas (Doric Lenses, Quebec, Canada) using Doric Lenses system controlled by Doric Neuroscience Studio version 5.3.

Video recording was time-locked with photometry signal while mice ambulated their home cage with cage top removed in a novel recording room. Signal processing was performed by a Doric Neuroscience Studio photometry analyzer. $\Delta F/F_0$ was calculated for the 405-nm and 465-nm channels independently using a least mean square fit, and then, $\Delta F/F_0$ (405 nm) was subtracted from $\Delta F/F_0$ (465 nm) to yield a corrected trace that was subsequently lowpass filtered at 2 Hz (45) to yield the final bulk calcium signal and $z$-normalized. Behavior in videos was manually annotated for exploratory rearing (centered around initial apogee) and the time of transition when mice started or stopped horizontal XY-plane movement ("stop to start" and "start to stop," respectively). Data analysis was performed using custom-written scripts in MATLAB R2019a (The MathWorks, Inc., Natick, MA).

## Statistical Analysis

To compare two groups, unpaired $t$ tests with Welch's correction or paired $t$ tests were used. To compare three or more groups, ordinary or repeated-measures one- or two-way analysis of variance with Sidak's multiple comparisons test was used. One-sample $t$ tests were used to compare experimental data with a DI = 0. $p < .05$ was considered significant. All tests were two-tailed, except for one-sample $t$ tests, which were one-tailed because of the clear unidirectional hypothesis that spatial memory manifests as DI > 0. Statistical analyses were performed in Prism 9 (GraphPad, San Diego, CA). Error bars depict standard error of the mean (SEM).

# RESULTS

## Targeting vMCs Projecting to the dDG

We exploited the well-organized distant bilateral axonal projection of vMCs to the IML of the dDG (Figure 1A) (27,29,46–48) to express proteins of interest in longitudinally projecting vMCs in wild-type mice. Retrograde-AAV-pgk-Cre was unilaterally infused into dDG, and Cre-dependent GCaMP6f was infused into the contralateral vDG hilus (Figure 1B). This resulted in the expression of GCaMP6f in large ventral hilar cells, with a band of GCaMP6f+ projections to the contralateral vDG and bilateral dDG IML (Figure 1C). Our stereotaxic coordinates for vMCs were selected to be consistent with previous functional studies of both vMCs (31) and vDG granule cells (49) and conform with a recent anatomical study of MC projections that defined the dDG as the rostral half of the DG (AP −1.0 to −2.5 mm) and the vDG as the caudal half of the DG (AP −2.7 to −4.0 mm) (50). Dorsal and vMCs differ in their expression of calretinin, which, in mice, is only expressed in vMCs (Figure S1) (29,30,51). Confirming that our targeting coordinates were consistent with previous definitions of vMCs, in the hilus, we found that approximately 87% of GCaMP6f+ neurons were also calretinin+, while approximately 68% of calretinin+ neurons were GCaMP6f+. We did identify low levels of GCaMP6f off-target expression in neighboring vDG granule cells and vCA3 pyramidal neurons (Figure 1D, E). Thus, these data show that this strategy is selective but not perfectly specific for vMCs, similar to other methods for MC targeting using D2-Cre (52,53) or Crlr-Cre (54) transgenic lines.

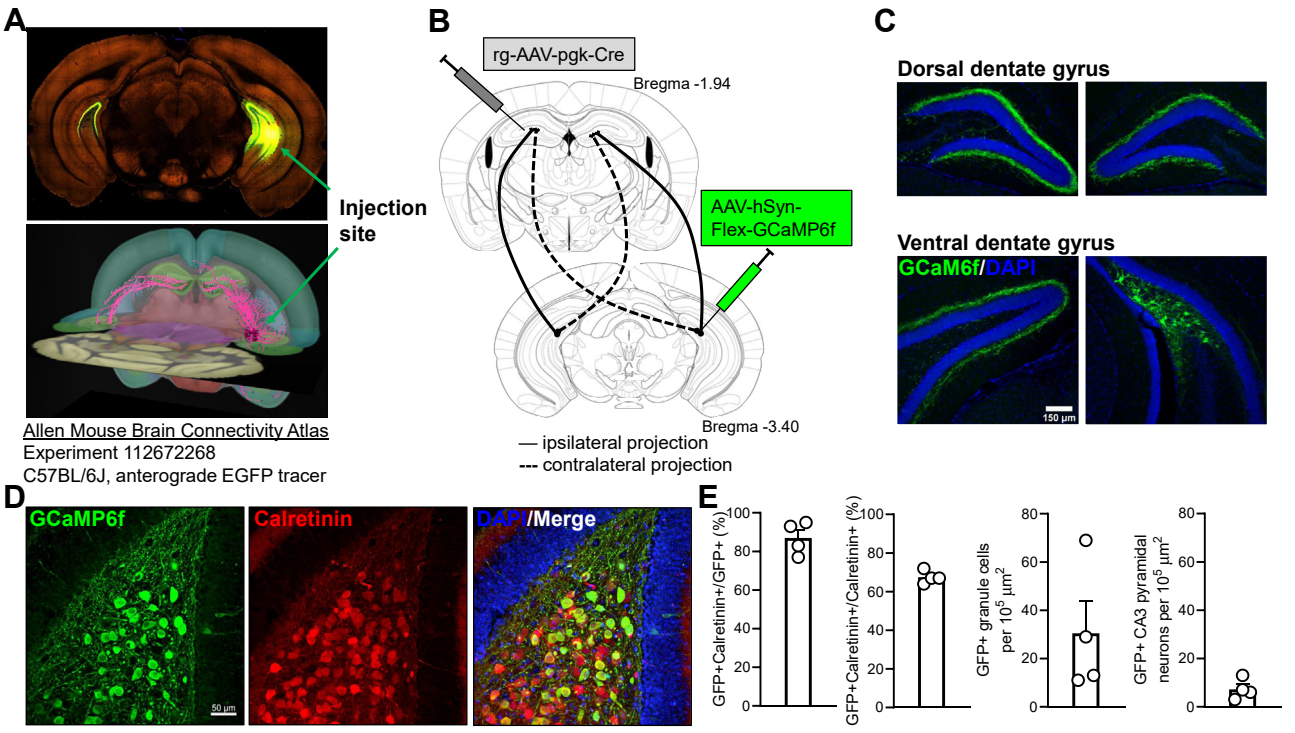


**Figure 1.** Intersectional targeting of longitudinal vMC projections. **(A)** vMC to dDG longitudinal circuit illustrated by the Allen Mouse Brain Connectivity Atlas (81). AAV expressing EGFP was infused into the ventral hilus of wild-type C57BL/6J mouse (top). Serial two-photon tomography shows axonal projections throughout longitudinal extent of the hippocampus, with strong projection to the dDG IML (https://connectivity.brain-map.org/projection/experiment/112672268). While this tracer is not specific for MCs, most of the depicted circuit comprises MC projections. **(B)** To target vMCs specifically, retrograde-AAV-pgk-Cre was infused into dDG IML, and AAV-hSyn-Flex-GCaMP6f was infused into contralateral vDG hilus, enabling recombination only in vMCs that project to dDG. **(C)** Fluorescence microscopy from CD-1 mouse following targeting strategy shown in panel **(B)** reveals GCaMP6f is expressed in vMC somata with organized projections to contralateral vDG and bilateral dDG. **(D)** GCaMP6f from targeting strategy in panel **(B)** is highly colocalized with calretinin, a marker for ventral but not dorsal MCs. **(E)** Quantification of viral targeting strategy in panel **(B)** from 4 mice reveals that most GCaMP6f+ hilar neurons are calretinin+, with limited off-target expression in nearby ventral granule cells and CA3 pyramidal neurons. AAV, adeno-associated virus; CA3, cornu ammonis 3; dDG, dorsal dentate gyrus; EGFP, enhanced green fluorescent protein; GFP, green fluorescent protein; IML, inner molecular layer; MC, mossy cell; vDG, ventral dentate gyrus; vMC, ventral MC.

## Activation of Longitudinally Projecting vMCs During Exploratory Rearing

While most in vivo studies of MC activity have focused on dMCs (55–57), recent work using microendoscopy showed that in aggregate, individual vMCs are significantly more active in novel environments than in familiar environments (33). To more granularly examine how vMC activity correlates with the animal's exploration of its environment, we used fiber photometry to record GCaMP6f calcium activity in vMCs (Figure 2A) during exploratory rearing events. Rearing on hind legs and horizontal exploration comprise an information gathering routine. Rearing but not horizontal movement rapidly changes the mouse's vantage point and multisensory inputs from local cues to more global environmental landmarks (58,59). Recent in vivo multichannel recordings showed large increases in medial perforant path input to the DG during rearing events as compared with horizontal running, and thus, while both behaviors involve information gathering, they may be differentially associated with vMC population activity (60). Consistent with this notion, we found that vMC activity increased concurrent with and immediately after rearing apogee (Figure 2B–D). We also tested whether vMC calcium activity was altered when mice initiated or stopped horizontal movement (Figure 2E, F). Neither was associated with substantial vMC activity. We calculated area under the curve of the calcium signal across mice for the 2 seconds before and after each behavior. While there was no difference in area under the curve between all three behaviors during the 2 seconds leading up to each behavior, there was a significant difference between rearing and both horizontal locomotor transitions in the 2 seconds immediately after the behavior (Figure 2G). Consistent with the findings by Fredes *et al.* (33), these results suggest that vMCs projecting to the dDG are active not only during exploration of an entirely novel environment (33) but also during individual bouts of rearing that are important for continual environmental mapping (60).

## Ventral MCs Functionally Target dDG Granule Cells

Electron microscopy has revealed that most vMC axonal synaptic targets in the dDG are on spines of granule cell dendrites in the IML (33,46,61). To test the functionality of this longitudinal circuit, we used AAV1 as an anterograde

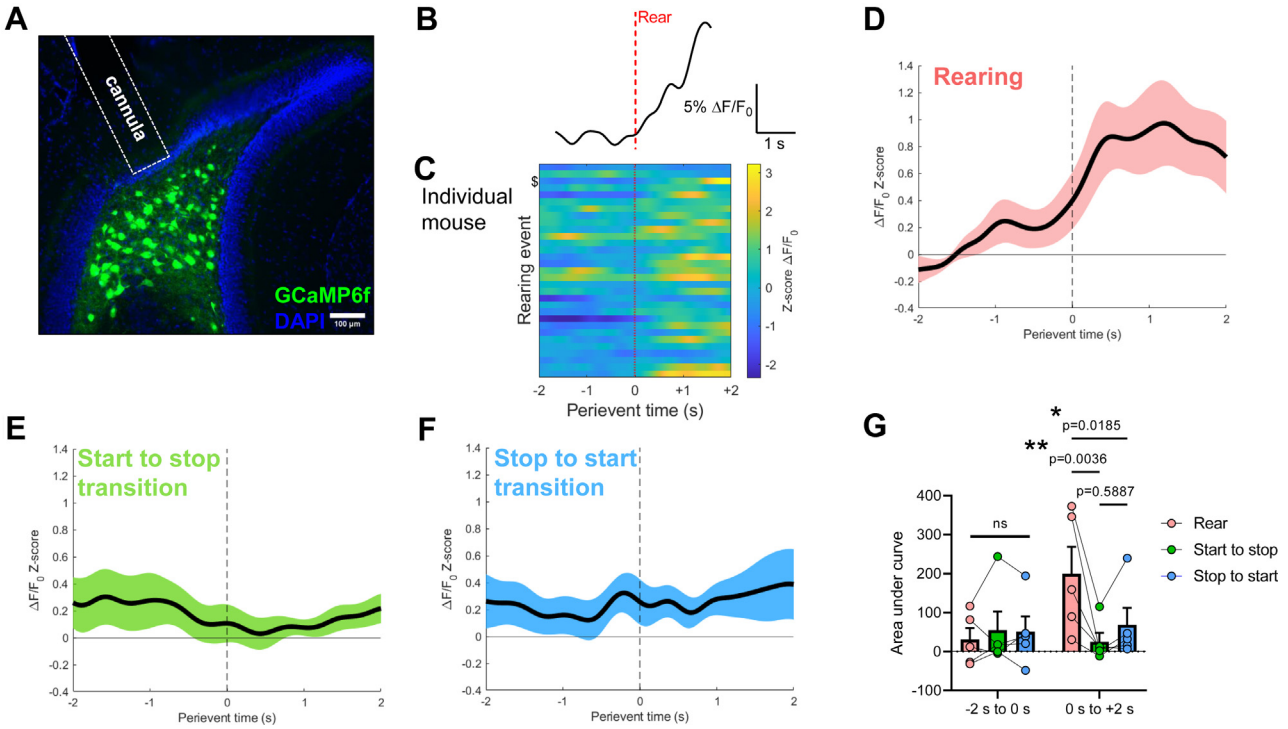


**Figure 2.** In vivo fiber photometry reveals that vMCs are selectively activated by exploratory rearing. **(A)** Fluorescence microscopy of GCaMP6f expression in vMCs by intersectional targeting and fiber optic cannula placement. **(B)** Example individual photometry trace surrounding an exploratory rearing event. Vertical red dashed line corresponds to initial rearing apogee. **(C)** $\Delta F/F_0$ *z* scores of rearing events aligned to time of initial rearing apogee in an individual mouse. Events are ordered chronologically during the recording. $ corresponds to trace in panel **(B)**. **(D)** $\Delta F/F_0$ *z* scores were aligned to time of rearing apogee (perievent time = 0), averaged within mouse, then averaged across mice (68 rearing events from 5 mice). Black line depicts mean $\Delta F/F_0$ *z* score, pink depicts SEM. **(E, F)** To test whether vMCs were activated by abrupt changes in motor behavior or nonrearing exploration, $\Delta F/F_0$ *z* scores for the same 5 mice from **(D)** during the same behavioral session were aligned to time when mice transitioned between XY-plane horizontal movement and no horizontal movement (E, start to stop, 98 transitions) or between no horizontal movement and XY-plane horizontal movement (F, stop to start, 98 transitions). Black line depicts mean $\Delta F/F_0$ *z* score; shading depicts SEM. **(G)** From the averaged $\Delta F/F_0$ *z*-score curves, area under the curve was calculated for the 2 seconds before (−2 to 0 s) and after (0 to +2 s) the indicated behavioral event, revealing that vMC calcium activity during rearing was greater than both horizontal motor transitions in the time period immediately after the behavior but not leading up to the behavior (time × behavior interaction: $F_{2,8} = 8.498$, $p = .011$; time: $F_{1,4} = 19.24$, $p = .012$; behavior: $F_{2,8} = 4.197$, $p = .057$). Pairwise comparison *p* values are shown in the figure. vMC, ventral mossy cell.

transsynaptic tracer of functional synapses (62,63). We infused AAV1-hSyn-Cre unilaterally into the ventral hilus to serve as the seed region and infused Cre-dependent mCherry (AAV-DIO-mCherry) into either ipsilateral or contralateral dDG to report Cre recombination (Figure 3A). AAV-DIO-mCherry infusion did not express mCherry in the absence of ventral hilar AAV1-Cre, suggesting that detectable fluorophore is due to Cre-mediated recombination and not leak expression (Figure 3B, left). The addition of AAV1-Cre in either the contralateral (Figure 3B, middle) or ipsilateral (Figure 3B, right) ventral hilus resulted in mCherry+ granule cells in the dDG, along with some labeling of dorsal hilar neurons. A limitation of this experiment is that it likely also captured longitudinally projecting vCA3c neurons (64), and AAV1 can also spread retrogradely, though with lower efficiency (62). We therefore expressed channelrhodopsin fused to mCherry in vMCs using the retrograde-AAV-Cre approach shown in Figure 1, whose terminals project to the dDG IML (Figure 3C). We performed whole-cell patch-clamp recordings from dDG granule cells while stimulating channelrhodopsin+ terminals (originating from vMCs) in the dorsal IML using 473-nm blue light at 20 Hz (Figure 3D) (50). Action potentials were detected in response to blue light upon depolarization of dDG granule cells membrane potential to approximately −60 mV (Figure 3E). These data support functional monosynaptic connectivity between vMCs and dDG granule cells and are consistent with recent reports showing functional connectivity from both vMCs to dDG granule cells (32,33) and conversely from dMCs to ventral granule cells (50). Furthermore, 0 of 9 mice expressing vMC channelrhodopsin-mCherry or mCherry alone showed projections to the medial prefrontal cortex (Figure S2).

## Chemogenetic Excitation of vMCs Activates dDG Granule Cells and Impairs Performance on a Test of Long-term Spatial Memory

We next aimed to model persistent activation of vMCs and test whether this vMC hyperactivation influences a behavior

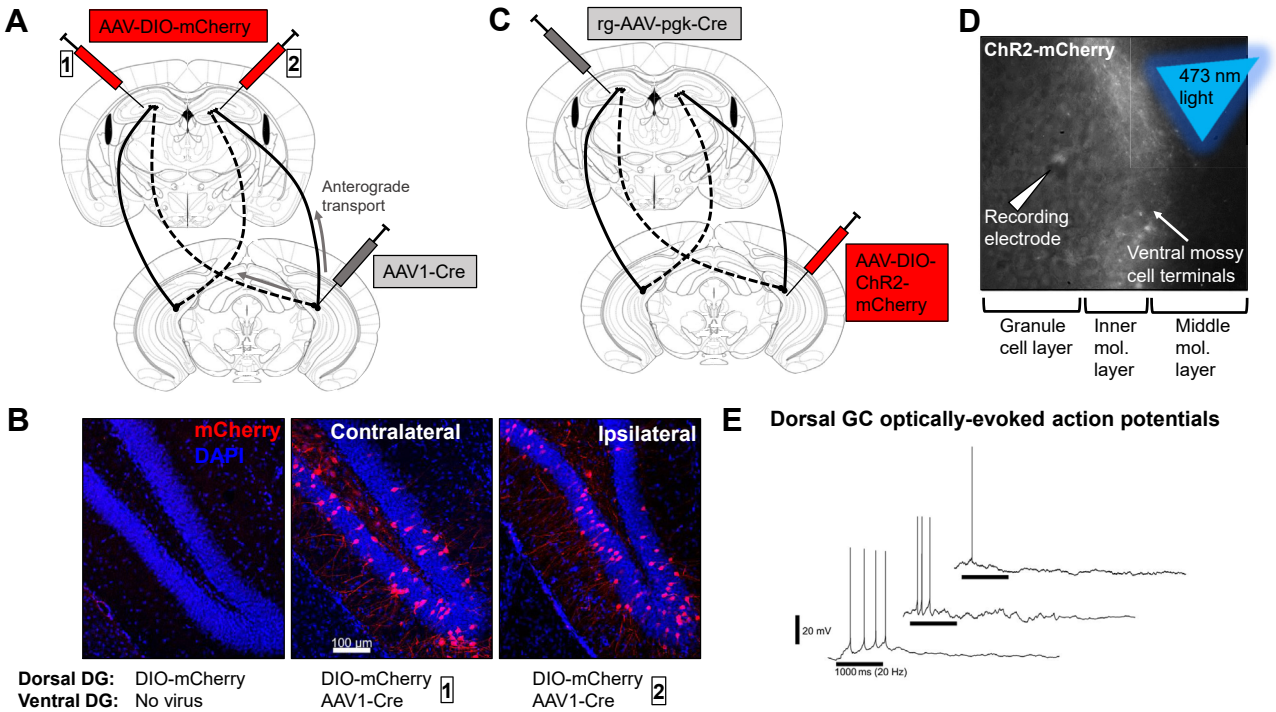


**Figure 3.** AAV1-mediated anterograde transsynaptic tracing and optogenetic excitation of vMC terminals reveals functional synapses between vMCs and dorsal granule cells. **(A)** AAV1-Cre was infused unilaterally into vDG hilus, and Cre-dependent mCherry (AAV-DIO-mCherry) was infused either contralaterally (box 1) or ipsilaterally (box 2) to dDG to detect anterograde transsynaptic trafficking. **(B)** AAV-DIO-mCherry does not express mCherry when infused alone (left); however, additional infusion of AAV1-Cre in either contralateral (middle) or ipsilateral (right) DG results in dDG granule cell expression of mCherry, supporting functional synaptic connectivity between the ventral hilus and dDG most consistent with longitudinal MC projections. **(C)** Channelrhodopsin-mCherry (AAV-EF1a-double floxed-hChR2(H134R)-mCherry-WPRE-HGHpA) was expressed in vMCs projecting to the contralateral dDG by intersectional targeting. **(D)** In slices, whole-cell patch-clamp recordings from dDG granule cells were performed while stimulating channelrhodopsin-mCherry-expressing vMC terminals in the dDG IML using a blue laser (473-nm wavelength, 5-ms pulse duration, 20 Hz for 1 s). **(E)** Action potentials were elicited from dDG granule cells held at approximately −60 mV (traces are shown for each of the three granule cells demonstrating action potentials out of five total recorded granule cells from 2 mice). A horizontal black bar for each trace denotes a 1000-ms duration, 20-Hz blue light stimulation period. AAV, adeno-associated virus; DG, dentate gyrus; dDG, dorsal DG; GC, genome copies; IML, inner molecular layer; MC, mossy cell; vDG, ventral DG; vMC, ventral MC.

dependent on the dHPC formation and dDG: long-term spatial learning and memory (34,35). We expressed the $G_q$-coupled DREADD construct hM3Dq-mCherry (39) or control mCherry in bilateral vMCs (Figure 4A, B). Whole-cell recordings from vMCs expressing hM3Dq or mCherry control mice showed a significantly greater inward current in hM3Dq-expressing vMCs after bath application of the DREADD-ligand 10-μM CNO compared with control mice (Figure 4C). To determine an appropriate dose of CNO for in vivo behavioral experiments, we systemically injected CNO and stained for c-Fos induced 90 minutes later. We observed low levels of c-Fos in vMCs expressing mCherry or hM3Dq after vehicle treatment or in mCherry-expressing vMCs after 10 mg/kg CNO treatment (Figure 4D). c-Fos expression was robustly increased in hM3Dq-expressing vMCs by 10 mg/kg CNO treatment. However, hM3Dq+CNO–treated mice also demonstrated dense c-Fos expression in neighboring granule cells and CA3 and CA1 neurons despite their not expressing hM3Dq, which is suggestive of overly high levels of activation and possible seizure activity. Indeed, a careful review of recorded behavior revealed myoclonic jerks in a subset of mice (data not shown). Reducing CNO to 1 mg/kg still significantly activated vMCs in hM3Dq-expressing MCs compared with mCherry-expressing vMCs (Figure 4E) but did not hyperactivate neighboring granule cells. Consistent with excitatory connectivity in vivo between vMCs and dDG granule cells, 1 mg/kg CNO modestly but significantly increased c-Fos expression in dDG granule cells (Figure 4F). Based on these studies, we selected 1 mg/kg CNO to examine the effects of vMC hyperactivation in behavioral assays.

To test how vMC chemogenetic activation affects long-term spatial learning and memory, we used an OLM test, which permits temporal separation of encoding and retrieval and specifically requires intact dHPC function (44,65). We focused on encoding because vMC inhibition impaired encoding but not retrieval in previous work (31). After several days of habituation to an arena containing spatial cues, mice investigated two identical objects (training session) and, 24 hours later, returned to the arena where one of the two objects was moved to a novel location. Intact spatial memory is manifested by more time spent investigating the novel- than familiar-located object during this test session. We confirmed that outbred mice showed robust long-term spatial memory in this paradigm, enabling sample size

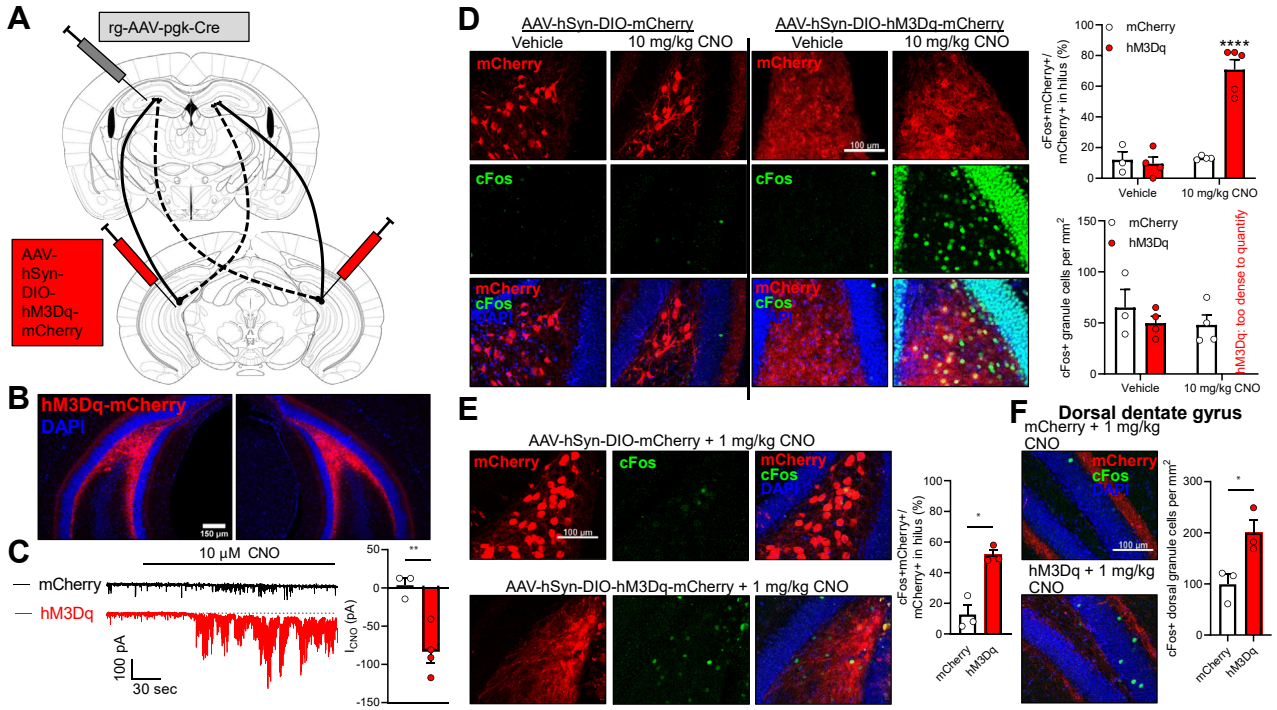


**Figure 4.** Chemogenetic activation of vMCs activates dorsal granule cells. **(A)** To express hM3Dq-mCherry or mCherry in vMCs, retrograde-AAV-pgk-Cre was unilaterally infused into dDG, and AAV-hSyn-DIO-hM3D(Gq)-mCherry or AAV-hSyn-DIO-mCherry was bilaterally infused into vDG hilus. **(B)** Fluorescence microscopy showing representative image of bilateral vMC targeting. **(C)** Whole-cell recordings from vMCs expressing either mCherry (3 cells from 2 mice) or hM3Dq-mCherry (4 cells from 3 mice) revealed that hM3Dq+ neurons showed significantly greater mean inward current after bath application of 10 micromolar CNO than control mCherry+ neurons. ($t_5 = 4.24$, $^{**}p = .0068$). **(D)** Mice with vMCs expressing mCherry ($n = 3$–4 mice) or hM3Dq-mCherry ($n = 4$–5 mice) were administered vehicle or 10 mg/kg CNO i.p., then perfused 90 minutes later and immunostained for c-Fos. Only vMCs expressing hM3Dq-mCherry strongly expressed c-Fos, but also strongly expressed c-Fos in neighboring vDG granule cells (treatment × virus: $F_{1,12} = 33.38$, $p < 10^{-4}$, $^{****}p < 10^{-4}$ vs. all other groups). **(E)** Same method as in panel **(D)** but with reduced dose of CNO (1 mg/kg) showed increase in c-Fos in vMCs expressing hM3Dq compared with mCherry ($n = 3$ mice per group; $t_{2.98} = 5.58$, $^{*}p = .012$), but no hyperactivation of neighboring granule cells. **(F)** dDG granule cell c-Fos was also significantly upregulated in mice with vMC expression of hM3Dq-mCherry treated with 1 mg/kg CNO as compared with mice with vMC expression of mCherry ($n = 3$ mice per group; $t_{3.77} = 3.21$, $^{*}p = .036$). CNO, clozapine N-oxide; dDG, dorsal dentate gyrus; vMC, ventral mossy cell; vDG, ventral DG.

estimates (Figure S3). We then treated mice expressing vMC hM3Dq or mCherry with 1 mg/kg CNO 30 minutes before the training session. Mice received no treatment during the testing session 24 hours later (Figure 5A). We did not detect training session differences in DI between mCherry and hM3Dq mice. However, 24 hours later, during the test session, mCherry mice showed significantly higher DI than hM3Dq mice, and only mCherry mice significantly differed from DI = 0 during the test session, supporting intact spatial memory (Figure 5B). Results appeared similar for unilaterally or bilaterally targeted vMCs (test DI mean ± SEM: mCherry: unilateral ($n = 2$): 0.31 ± 0.078, bilateral ($n = 8$): 0.19 ± 0.12; hM3Dq: unilateral ($n = 3$): 0.00 ± 0.060, bilateral ($n = 6$): −0.05 ± 0.090). The total duration of time spent investigating the objects did not significantly differ between virus groups during training or testing sessions (Figure 5C), arguing against changes in arousal or exploration preferences explaining the spatial memory deficit. In a 10-minute open field test (Figure 5D), there were no significant differences in total distance traveled or time in the arena center between virus groups (Figure 5E, F). The total number of rearing events also did not differ between groups (Figure 5G). Taken together, these data suggest that hyperactivation of vMCs during the training session impairs subsequent discrimination of a novel location from a familiar location without changing locomotor or exploratory behaviors.

## DISCUSSION

In this study, we identified behavioral correlates associated with vMC endogenous activation and quantified the effects of vMC chemogenetic activation on dDG granule cell excitation and dHPC-dependent long-term memory. We found that 1) vMCs in vivo are activated during exploratory rearing but not during horizontal exploration, 2) vMCs make functional excitatory synapses with dDG granule cells, and 3) chemogenetic activation of vMCs modestly activates dDG granule cells in vivo and impairs long-term spatial memory without significantly altering locomotor or exploratory behaviors. These data complement another recent study showing vMC activation by novel environments independent of locomotor activity, a significant excitatory effect of vMCs on dDG granule cells, and that chemogenetic activation of vMCs modifies contextual memory acquisition (33).

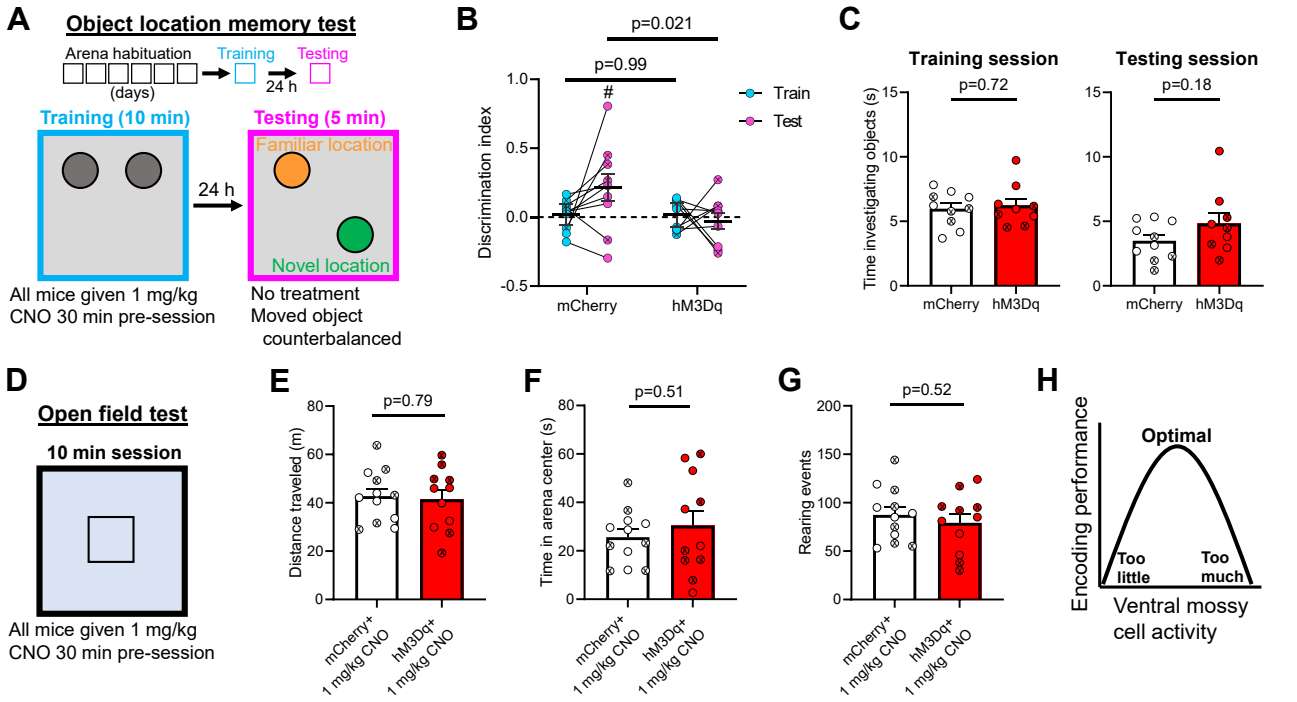


**Figure 5.** vMC hyperactivation during object location training impairs retrieval 24 hours later. **(A)** Schematic of the object location memory test. After 3 days of handling, mice undergo 6 days of habituation to an arena with spatial cues on the wall. The following day, they undergo a 10-minute training session, during which, they are exposed to two identical objects. Twenty-four hours later, they are returned to the arena for a 5-minute testing session where one object has been moved to a novel location and the other remains in the familiar location. CNO (1 mg/kg) was administered 30 minutes before the training session only. **(B)** CNO administration during training impaired object location memory in mice expressing hM3Dq in vMCs ($n$ = 10 mCherry, $n$ = 9 hM3Dq; virus × session: $F_{1,17}$ = 3.147, $p$ = .094; virus: $F_{1,17}$ = 4.338, $p$ = .053; session: $F_{1,17}$ = 1.192, $p$ = .29). Pairwise comparison p values are shown in the figure. One-sample $t$ test vs. DI = 0: $t_9$ = 2.20, #$p$ = .028. **(C)** Total time spent investigating both objects did not significantly differ between the mice expressing mCherry ($n$ = 10) or hM3Dq ($n$ = 9) during the training (left; $t_{15.65}$ = 0.37, $p$ = .72) or testing session (right; $t_{12.65}$ = 1.40, $p$ = .18). **(D–G)** Mice were later tested in a 10-minute open field test in an arena with a novel floor surface 30 minutes after administration of 1 mg/kg CNO ($n$ = 12 mCherry, $n$ = 11 hM3Dq) **(D)**. There was no significant difference between mCherry- and hM3Dq-expressing mice in the total distance traveled ($t_{19.74}$ = 0.27, $p$ = .79) **(E)**, time spent in the arena center ($t_{15.13}$ = 0.68, $p$ = .51) **(F)**, or number of rearing events ($t_{20.31}$ = 0.66, $p$ = .52) **(G)**. For panels **(B)** and **(C)** and **(E)–(G)**, individual data points containing "X" represent female mice. No mice were excluded because of lack of vMC targeting. **(H)** Schematic suggesting that a specific setpoint of vMC activity exists for optimal encoding performance, which is supported by previous work showing that inhibition of vMCs impairs spatial encoding (31) and this study suggesting that hyperactivation of vMCs also impairs spatial encoding. CNO, clozapine N-oxide; DI, discrimination index; vMC, ventral mossy cell.

Together, these studies suggest that vMCs in vivo respond to novel or updated environmental stimuli, and vMC activity has functional effects on dHPC-dependent cognitive processes.

Because MCs target both granule cells (direct pathway) and interneurons that inhibit granule cells (indirect pathway), considerable work has addressed whether the net effect of MC activation is to excite or inhibit DG granule cells, often with a translational interest in seizure generation and propagation (25,26,31,32,54,66–69). Distinctions between vMCs and dMCs are supported by physiological (33,70–72), biochemical (29,30), and anatomical (33,50,73) evidence, and some (31,33) but not all (32) studies suggest that the net physiological or functional action of MCs on dDG granule cells differs across the dorsoventral axis. There is also growing interest in the role of MCs relevant to behaviors affected in neuropsychiatric disorders, especially cognition (31,33,54,69). Interestingly, MCs may have different effects on short-term versus long-term spatial memory. When dMCs or vMCs are inhibited (31) or vMCs activated (this study) during the training session of the OLM, retrieval in a test session 24 hours later is reduced. However, a recent study targeting MCs across the dorsoventral axis reported that neither chemogenetic inhibition nor activation during OLM training impaired retrieval in a test session 1 hour later (69), highlighting differential participation in these two forms of memory with known mechanistic differences (74).

That either vMC activation or inhibition during OLM training impairs spatial memory after 24 hours supports an overall model that bidirectional perturbation of vMC activity, either too much or too little, impairs spatial encoding (Figure 5H), without influencing exploratory or locomotor behavior itself. Either ventral MC inhibition or strong activation may result in granule cell activation, depending on the balance between direct and indirect pathways (75). The point of convergence is likely dDG granule cells, as activation or inhibition of dDG but not of vDG granule cells impairs contextual encoding (49), and dDG granule cells provide a long-term stable representation of space (76). While vMC activation may impair spatial encoding, another possibility for our OLM results is impaired updating of

the new spatial representation of the arena with new objects during the training session. Relatedly, our findings may be confounded by state dependency, whereby CNO administration during OLM training but not during habituation influenced a change in general affective or cognitive state. Finally, it is important to acknowledge that without manipulation specifically of vMC projections within the dHPC, our data cannot support a claim that hyperactivation of this projection is causal for the observed spatial memory deficit.

Our results and those of others suggest that long axis intrahippocampal projections such as vMC to dDG potentially have functional relevance in systems where their activity is altered bidirectionally. It is unknown whether MC number or activity is changed in psychosis, and we want to be clear that future work using rodent models with genetic or environmental insults leading to vHPC hyperactivity is required to directly test the question of whether anterior/ventral HPC hyperactivity in the cornu ammonis leads to increased vMC activity or whether vMC manipulation may mitigate dHPC cognitive dysfunction in these models. Area CA4 volume by neuroimaging is reduced in living people with schizophrenia (77), and schizophrenia postmortem studies have also shown cellular and biochemical changes in CA4 (78–80). Thus, one important goal for future postmortem work would be to differentiate MCs more specifically from other cell types in this heterogeneous region. Finally, our and others' manipulations of vMCs were acute using adult mice, which is notable because cognitive effects after MC ablation are transient (54). Future studies should test how chronic manipulations of vMC activity influence different spatial memory paradigms as well as whether effects differ during neurodevelopment.

## ACKNOWLEDGMENTS AND DISCLOSURES

This work was supported by the National Institutes of Health (NIH) (Grant Nos. MH116339 [to ASL] and NS107424 [to CZ]), the Nicholas Hobbs Discovery Grant (to ASL), and the Vanderbilt Department of Psychiatry and Behavioral Sciences. Experiments and data analysis were performed in part using the Vanderbilt University Medical Center Cell Imaging Shared Resource (supported by NIH Grant Nos. CA68485, DK20593, DK58404, DK59637, and EY08126). The content is solely the responsibility of the authors and does not necessarily represent the official views of the NIH.

We thank Marina Picciotto, Ph.D., and Ye Han, Ph.D., for helpful comments on this work.

A previous version of this article was published as a preprint on bioRxiv: https://www.biorxiv.org/content/10.1101/2020.12.15.422938v2.

PJC receives research support from Lundbeck Pharmaceuticals and Boehringer Ingelheim and is an inventor on multiple patents for allosteric modulators for several classes of metabotropic glutamate receptors. All other authors report no biomedical financial interests or potential conflicts of interest.

## ARTICLE INFORMATION

From the Department of Psychiatry and Behavioral Sciences (JPB, SLR, WK, LS, ASL), Department of Neurology (CZ, ASL), and Vanderbilt Kennedy Center (PJC, ASL), Vanderbilt University Medical Center; and Warren Center for Neuroscience Drug Discovery (MEJ, PJC), Department of Pharmacology (MEJ, PJC), Quantitative and Chemical Biology Program (JQ), Vanderbilt Brain Institute (CZ, PJC, ASL), and Vanderbilt Center for Addiction Research (MEJ, PJC, ASL), Vanderbilt University, Nashville, Tennessee.

Address correspondence to Alan S. Lewis, M.D., Ph.D., at alan.s.lewis@vumc.org.

Received Feb 3, 2021; revised Apr 21, 2021; accepted Apr 23, 2021.

Supplementary material cited in this article is available online at https://doi.org/10.1016/j.bpsgos.2021.04.005.

## REFERENCES

1. Schobel SA, Chaudhury NH, Khan UA, Paniagua B, Styner MA, Asllani I, *et al.* (2013): Imaging patients with psychosis and a mouse model establishes a spreading pattern of hippocampal dysfunction and implicates glutamate as a driver. Neuron 78:81–93.
2. Schobel SA, Kelly MA, Corcoran CM, Van Heertum K, Seckinger R, Goetz R, *et al.* (2009): Anterior hippocampal and orbitofrontal cortical structural brain abnormalities in association with cognitive deficits in schizophrenia. Schizophr Res 114:110–118.
3. McHugo M, Talati P, Woodward ND, Armstrong K, Blackford JU, Heckers S (2018): Regionally specific volume deficits along the hippocampal long axis in early and chronic psychosis. Neuroimage Clin 20:1106–1114.
4. Szeszko PR, Goldberg E, Gunduz-Bruce H, Ashtari M, Robinson D, Malhotra AK, *et al.* (2003): Smaller anterior hippocampal formation volume in antipsychotic-naive patients with first-episode schizophrenia. Am J Psychiatry 160:2190–2197.
5. McHugo M, Armstrong K, Roeske MJ, Woodward ND, Blackford JU, Heckers S (2020): Hippocampal volume in early psychosis: A 2-year longitudinal study. Transl Psychiatry 10:306.
6. McHugo M, Talati P, Armstrong K, Vandekar SN, Blackford JU, Woodward ND, Heckers S (2019): Hyperactivity and reduced activation of anterior hippocampus in early psychosis. Am J Psychiatry 176:1030–1038.
7. Talati P, Rane S, Kose S, Blackford JU, Gore J, Donahue MJ, Heckers S (2014): Increased hippocampal CA1 cerebral blood volume in schizophrenia. Neuroimage Clin 5:359–364.
8. Schobel SA, Lewandowski NM, Corcoran CM, Moore H, Brown T, Malaspina D, Small SA (2009): Differential targeting of the CA1 subfield of the hippocampal formation by schizophrenia and related psychotic disorders. Arch Gen Psychiatry 66:938–946.
9. Modinos G, Şimşek F, Azis M, Bossong M, Bonoldi I, Samson C, *et al.* (2018): Prefrontal GABA levels, hippocampal resting perfusion and the risk of psychosis. Neuropsychopharmacology 43:2652–2659.
10. Tregellas JR, Smucny J, Harris JG, Olincy A, Maharajh K, Kronberg E, *et al.* (2014): Intrinsic hippocampal activity as a biomarker for cognition and symptoms in schizophrenia. Am J Psychiatry 171:549–556.
11. Francis MM, Hummer TA, Vohs JL, Yung MG, Liffick E, Mehdiyoun NF, *et al.* (2016): Functional neuroanatomical correlates of episodic memory impairment in early phase psychosis. Brain Imaging Behav 10:1–11.
12. Ragland JD, Layher E, Hannula DE, Niendam TA, Lesh TA, Solomon M, *et al.* (2016): Impact of schizophrenia on anterior and posterior hippocampus during memory for complex scenes. Neuroimage Clin 13:82–88.
13. Avery SN, McHugo M, Armstrong K, Blackford JU, Woodward ND, Heckers S (2019): Disrupted habituation in the early stage of psychosis. Biol Psychiatry Cogn Neurosci Neuroimaging 4:1004–1012.
14. Holt DJ, Weiss AP, Rauch SL, Wright CI, Zalesak M, Goff DC, *et al.* (2005): Sustained activation of the hippocampus in response to fearful faces in schizophrenia. Biol Psychiatry 57:1011–1019.
15. Ragland JD (2019): Relating basal and phasic hippocampal activity in people with psychosis: A translational bridge to understanding memory deficits? Am J Psychiatry 176:979–981.
16. Bast T, Pezze M, McGarrity S (2017): Cognitive deficits caused by prefrontal cortical and hippocampal neural disinhibition. Br J Pharmacol 174:3211–3225.
17. Kätzel D, Wolff AR, Bygrave AM, Bannerman DM (2020): Hippocampal hyperactivity as a druggable circuit-level origin of aberrant salience in schizophrenia. Front Pharmacol 11:486811.
18. Grace AA (2012): Dopamine system dysregulation by the hippocampus: Implications for the pathophysiology and treatment of schizophrenia. Neuropharmacology 62:1342–1348.

19. Spellman T, Rigotti M, Ahmari SE, Fusi S, Gogos JA, Gordon JA (2015): Hippocampal–prefrontal input supports spatial encoding in working memory. Nature 522:309–314.
20. Jones MW, Wilson MA (2005): Theta rhythms coordinate hippocampal-prefrontal interactions in a spatial memory task. PLoS Biol 3:e402.
21. Hyman JM, Zilli EA, Paley AM, Hasselmo ME (2010): Working memory performance correlates with prefrontal-hippocampal theta interactions but not with prefrontal neuron firing rates. Front Integr Neurosci 4:2.
22. Sigurdsson T, Stark KL, Karayiorgou M, Gogos JA, Gordon JA (2010): Impaired hippocampal-prefrontal synchrony in a genetic mouse model of schizophrenia. Nature 464:763–767.
23. O'Neill PK, Gordon JA, Sigurdsson T (2013): Theta oscillations in the medial prefrontal cortex are modulated by spatial working memory and synchronize with the hippocampus through its ventral subregion. J Neurosci 33:14211–14224.
24. Wolff AR, Bygrave AM, Sanderson DJ, Boyden ES, Bannerman DM, Kullmann DM, Kätzel D (2018): Optogenetic induction of the schizophrenia-related endophenotype of ventral hippocampal hyperactivity causes rodent correlates of positive and cognitive symptoms. Sci Rep 8:12871.
25. Scharfman HE (2016): The enigmatic mossy cell of the dentate gyrus. Nat Rev Neurosci 17:562–575.
26. Scharfman HE, Myers CE (2013): Hilar mossy cells of the dentate gyrus: A historical perspective. Front Neural Circuits 6:106.
27. Ribak CE, Seress L, Amaral DG (1985): The development, ultrastructure and synaptic connections of the mossy cells of the dentate gyrus. J Neurocytol 14:835–857.
28. Frotscher M, Seress L, Schwerdtfeger WK, Buhl E (1991): The mossy cells of the fascia dentata: A comparative study of their fine structure and synaptic connections in rodents and primates. J Comp Neurol 312:145–163.
29. Blasco-Ibáñez JM, Freund TF (1997): Distribution, ultrastructure, and connectivity of calretinin-immunoreactive mossy cells of the mouse dentate gyrus. Hippocampus 7:307–320.
30. Fujise N, Liu Y, Hori N, Kosaka T (1998): Distribution of calretinin immunoreactivity in the mouse dentate gyrus: II. Mossy cells, with special reference to their dorsoventral difference in calretinin immunoreactivity. Neuroscience 82:181–200.
31. Bui AD, Nguyen TM, Limouse C, Kim HK, Szabo GG, Felong S, *et al.* (2018): Dentate gyrus mossy cells control spontaneous convulsive seizures and spatial memory. Science 359:787–790.
32. Bernstein HL, Lu Y-L, Botterill JJ, Duffy ÁM, LaFrancois JJ, Scharfman HE (2020): Excitatory effects of dentate gyrus mossy cells and their ability to influence granule cell firing: An optogenetic study in adult mouse hippocampal slices. bioRxiv. https://doi.org/10.1101/2020.06.06.137844.
33. Fredes F, Silva MA, Koppensteiner P, Kobayashi K, Joesch M, Shigemoto R (2021): Ventro-dorsal hippocampal pathway gates novelty-induced contextual memory formation. Curr Biol 31:25–38.e5.
34. Moser E, Moser MB, Andersen P (1993): Spatial learning impairment parallels the magnitude of dorsal hippocampal lesions, but is hardly present following ventral lesions. J Neurosci 13:3916–3925.
35. Moser MB, Moser EI, Forrest E, Andersen P, Morris RG (1995): Spatial learning with a minislab in the dorsal hippocampus. Proc Natl Acad Sci U S A 92:9697–9701.
36. Scharfman HE, Schwartzkroin PA (1988): Electrophysiology of morphologically identified mossy cells of the dentate hilus recorded in guinea pig hippocampal slices. J Neurosci 8:3812–3821.
37. Tuttle AH, Philip VM, Chesler EJ, Mogil JS (2018): Comparing phenotypic variation between inbred and outbred mice. Nat Methods 15:994–996.
38. Chen TW, Wardill TJ, Sun Y, Pulver SR, Renninger SL, Baohan A, *et al.* (2013): Ultrasensitive fluorescent proteins for imaging neuronal activity. Nature 499:295–300.
39. Krashes MJ, Koda S, Ye C, Rogan SC, Adams AC, Cusher DS, *et al.* (2011): Rapid, reversible activation of AgRP neurons drives feeding behavior in mice. J Clin Invest 121:1424–1428.
40. Liu W, Davis RL (2014): Calretinin and calbindin distribution patterns specify subpopulations of type I and type II spiral ganglion neurons in postnatal murine cochlea. J Comp Neurol 522:2299–2318.
41. Zhou QG, Nemes AD, Lee D, Ro EJ, Zhang J, Nowacki AS, *et al.* (2019): Chemogenetic silencing of hippocampal neurons suppresses epileptic neural circuits. J Clin Invest 129:310–323.
42. Zhou C, Huang Z, Ding L, Deel ME, Arain FM, Murray CR, *et al.* (2013): Altered cortical GABAA receptor composition, physiology, and endocytosis in a mouse model of a human genetic absence epilepsy syndrome. J Biol Chem 288:21458–21472.
43. Zhou C, Lippman JJ, Sun H, Jensen FE (2011): Hypoxia-induced neonatal seizures diminish silent synapses and long-term potentiation in hippocampal CA1 neurons. J Neurosci 31:18211–18222.
44. Vogel-Ciernia A, Wood MA (2014): Examining object location and object recognition memory in mice. Curr Protoc Neurosci 69:8.31.1–8.31.17.
45. Zalocusky KA, Ramakrishnan C, Lerner TN, Davidson TJ, Knutson B, Deisseroth K (2016): Nucleus accumbens D2R cells signal prior outcomes and control risky decision-making. Nature 531:642–646.
46. Buckmaster PS, Wenzel HJ, Kunkel DD, Schwartzkroin PA (1996): Axon arbors and synaptic connections of hippocampal mossy cells in the rat in vivo. J Comp Neurol 366:271–292.
47. Buzsàki G, Eidelberg E (1981): Commissural projection to the dentate gyrus of the rat: Evidence for feed-forward inhibition. Brain Res 230:346–350.
48. Laurberg S, Sørensen KE (1981): Associational and commissural collaterals of neurons in the hippocampal formation (hilus fasciae dentatae and subfield CA3). Brain Res 212:287–300.
49. Kheirbek MA, Drew LJ, Burghardt NS, Costantini DO, Tannenholz L, Ahmari SE, *et al.* (2013): Differential control of learning and anxiety along the dorsoventral axis of the dentate gyrus. Neuron 77:955–968.
50. Houser CR, Peng Z, Wei X, Huang CS, Mody I (2021): Mossy cells in the dorsal and ventral dentate gyrus differ in their patterns of axonal projections. J Neurosci 41:991–1004.
51. Liu Y, Fujise N, Kosaka T (1996): Distribution of calretinin immunoreactivity in the mouse dentate gyrus. I. General description. Exp Brain Res 108:389–403.
52. Gangarossa G, Longueville S, De Bundel D, Perroy J, Hervé D, Girault JA, Valjent E (2012): Characterization of dopamine D1 and D2 receptor-expressing neurons in the mouse hippocampus. Hippocampus 22:2199–2207.
53. Puighermanal E, Biever A, Espallergues J, Gangarossa G, De Bundel D, Valjent E (2015): drd2-cre:ribotag mouse line unravels the possible diversity of dopamine d2 receptor-expressing cells of the dorsal mouse hippocampus. Hippocampus 25:858–875.
54. Jinde S, Zsiros V, Jiang Z, Nakao K, Pickel J, Kohno K, *et al.* (2012): Hilar mossy cell degeneration causes transient dentate granule cell hyperexcitability and impaired pattern separation. Neuron 76:1189–1200.
55. Danielson NB, Turi GF, Ladow M, Chavlis S, Petrantonakis PC, Poirazi P, *et al.* (2017): In vivo imaging of dentate gyrus mossy cells in behaving mice. Neuron 93:552–559.e4.
56. GoodSmith D, Chen X, Wang C, Kim SH, Song H, Burgalossi A, *et al.* (2017): Spatial representations of granule cells and mossy cells of the dentate gyrus. Neuron 93:677–e690.e5.
57. Senzai Y, Buzsáki G (2017): Physiological properties and behavioral correlates of hippocampal granule cells and mossy cells. Neuron 93:691–704.e5.
58. Knierim JJ, Hamilton DA (2011): Framing spatial cognition: Neural representations of proximal and distal frames of reference and their roles in navigation. Physiol Rev 91:1245–1279.
59. Lever C, Burton S, O'Keefe J (2006): Rearing on hind legs, environmental novelty, and the hippocampal formation. Rev Neurosci 17:111–133.
60. Barth AM, Domonkos A, Fernandez-Ruiz A, Freund TF, Varga V (2018): Hippocampal network dynamics during rearing episodes. Cell Rep 23:1706–1715.

61. Wenzel HJ, Buckmaster PS, Anderson NL, Wenzel ME, Schwartzkroin PA (1997): Ultrastructural localization of neurotransmitter immunoreactivity in mossy cell axons and their synaptic targets in the rat dentate gyrus. Hippocampus 7:559–570.
62. Zingg B, Chou XL, Zhang ZG, Mesik L, Liang F, Tao HW, Zhang LI (2017): AAV-mediated anterograde transsynaptic tagging: Mapping corticocollicular input-defined neural pathways for defense behaviors. Neuron 93:33–47.
63. Zingg B, Peng B, Huang J, Tao HW, Zhang LI (2020): Synaptic specificity and application of anterograde transsynaptic AAV for probing neural circuitry. J Neurosci 40:3250–3267.
64. Li XG, Somogyi P, Ylinen A, Buzsáki G (1994): The hippocampal CA3 network: An in vivo intracellular labeling study. J Comp Neurol 339:181–208.
65. Haettig J, Stefanko DP, Multani ML, Figueroa DX, McQuown SC, Wood MA (2011): HDAC inhibition modulates hippocampus-dependent long-term memory for object location in a CBP-dependent manner. Learn Mem 18:71–79.
66. Botterill JJ, Lu YL, LaFrancois JJ, Bernstein HL, Alcantara-Gonzalez D, Jain S, *et al.* (2019): An excitatory and epileptogenic effect of dentate gyrus mossy cells in a mouse model of epilepsy. Cell Rep 29:2875–2889.e6.
67. Scharfman HE (1995): Electrophysiological evidence that dentate hilar mossy cells are excitatory and innervate both granule cells and interneurons. J Neurophysiol 74:179–194.
68. Hsu TT, Lee CT, Tai MH, Lien CC (2016): Differential recruitment of dentate gyrus interneuron types by commissural versus perforant pathways. Cereb Cortex 26:2715–2727.
69. Botterill JJ, Vinod KY, Gerencer KJ, Teixeira CM, LaFrancois JJ, Scharfman HE (2021): Bidirectional regulation of cognitive and anxiety-like behaviors by dentate gyrus mossy cells in male and female mice. J Neurosci 41:2475–2495.
70. Jinno S, Ishizuka S, Kosaka T (2003): Ionic currents underlying rhythmic bursting of ventral mossy cells in the developing mouse dentate gyrus. Eur J Neurosci 17:1338–1354.
71. Moretto JN, Duffy ÁM, Scharfman HE (2017): Acute restraint stress decreases c-fos immunoreactivity in hilar mossy cells of the adult dentate gyrus. Brain Struct Funct 222:2405–2419.
72. Duffy AM, Schaner MJ, Chin J, Scharfman HE (2013): Expression of c-fos in hilar mossy cells of the dentate gyrus in vivo. Hippocampus 23:649–655.
73. Botterill JJ, Gerencer KJ, Vinod KY, Alcantara-Gonzalez D, Scharfman HE (2021): Dorsal and ventral mossy cells differ in their axonal projections throughout the dentate gyrus of the mouse hippocampus. Hippocampus 31:522–539.
74. Vogel-Ciernia A, Matheos DP, Barrett RM, Kramár EA, Azzawi S, Chen Y, *et al.* (2013): The neuron-specific chromatin regulatory subunit BAF53b is necessary for synaptic plasticity and memory. Nat Neurosci 16:552–561.
75. Yeh CY, Asrican B, Moss J, Quintanilla LJ, He T, Mao X, *et al.* (2018): Mossy cells control adult neural stem cell quiescence and maintenance through a dynamic balance between direct and indirect pathways. Neuron 99:493–510.e4.
76. Hainmueller T, Bartos M (2018): Parallel emergence of stable and dynamic memory engrams in the hippocampus. Nature 558:292–296.
77. Nakahara S, Turner JA, Calhoun VD, Lim KO, Mueller B, Bustillo JR, *et al.* (2020): Dentate gyrus volume deficit in schizophrenia. Psychol Med 50:1267–1277.
78. Roeske MJ, Konradi C, Heckers S, Lewis AS (2020): Hippocampal volume and hippocampal neuron density, number and size in schizophrenia: A systematic review and meta-analysis of postmortem studies [published online ahead of print Jul 28]. Mol Psychiatry.
79. Harrison PJ, Law AJ, Eastwood SL (2003): Glutamate receptors and transporters in the hippocampus in schizophrenia. Ann N Y Acad Sci 1003:94–101.
80. Harrison PJ (2004): The hippocampus in schizophrenia: A review of the neuropathological evidence and its pathophysiological implications. Psychopharmacology (Berl) 174:151–162.
81. Oh SW, Harris JA, Ng L, Winslow B, Cain N, Mihalas S, *et al.* (2014): A mesoscale connectome of the mouse brain. Nature 508:207–214.